Numerical Simulations of Typhoon Morakot (2009) Using a Multiply Nested Tropical Cyclone Prediction Model

ERIC A. HENDRICKS,* YI JIN, JONATHAN R. MOSKAITIS, JAMES D. DOYLE, AND MELINDA S. PENG

Marine Meteorology Division, Naval Research Laboratory, Monterey, California

CHUN-CHIEH WU AND HUNG-CHI KUO

Department of Atmospheric Sciences, National Taiwan University, Taipei, Taiwan

(Manuscript received 15 January 2015, in final form 20 August 2015)

ABSTRACT

High-impact Typhoon Morakot (2009) was investigated using a multiply nested regional tropical cyclone prediction model. In the numerical simulations, the horizontal grid spacing, cumulus parameterizations, and microphysical parameterizations were varied, and the sensitivity of the track, intensity, and quantitative precipitation forecasts (QPFs) was examined. With regard to horizontal grid spacing, it is found that convective-permitting (5 km) resolution is necessary for a reasonably accurate QPF, while little benefit is gained through the use of a fourth domain at 1.67-km horizontal resolution. Significant sensitivity of the track forecast was found to the cumulus parameterization, which impacted the model QPFs. In particular, the simplified Arakawa–Schubert parameterization tended to erroneously regenerate the remnants of Tropical Storm Goni to the southwest of Morakot, affecting the large-scale steering flow and the track of Morakot. Strong sensitivity of the QPFs to the microphysical parameterization was found, with the track and intensity showing little sensitivity. It is also found that Morakot's accumulated precipitation was reasonably predictable, with the control simulation producing an equitable threat score of 0.56 for the 3-day accumulated precipitation using a threshold of 500 mm. This high predictability of precipitation is due in part to more predictable large-scale and topographic forcing.

1. Introduction

Typhoon Morakot (2009) was the deadliest typhoon to strike Taiwan in recorded history. The slow movement of Morakot over Taiwan, combined with its interaction with the southwesterly monsoon flow after landfall, produced tremendous amounts of precipitation (in excess of 2500 mm) over the southwestern portion of the island. The massive amounts of precipitation triggered a mudslide, destroying the village of Siao-Lin, and killing 500 people. In response to the disaster, a special workshop was held in Taipei, Taiwan, in 2010 to address deficiencies in the prediction of Morakot and its impacts, and the results were summarized in a number of papers published in the journal *Terrestrial, Atmospheric and Oceanic Sciences* (Wu 2013).

Considering the enormous impact of Morakot, a number of recent studies have examined various aspects of the storm. The studies range from its interaction with the southwest monsoon (Wu et al. 2011; Liang et al. 2011), initialization and data assimilation (Nguyen and Chen 2011; Schwartz et al. 2012), its interaction with orography (Fang et al. 2011; Xie and Zhang 2012), its very slow translational speed (Chien and Kuo 2011; Yen et al. 2011), and its operational prediction (Hendricks et al. 2011), to aspects of its internal structure and impact on precipitation (Wang et al. 2012; Hall et al. 2013). An overriding aspect of these studies is the complicated multiscale interactions at play and interaction with Taiwan's steep and complex orography (Wu and Kuo 1999) leading to the tremendous precipitation amounts. The steep terrain of Taiwan's Central Mountain Range

* Current affiliation: Department of Meteorology, Naval Postgraduate School, Monterey, California.

Corresponding author address: Eric A. Hendricks, Dept. of Meteorology, Naval Postgraduate School, Rm. 255, 589 Dyer Rd., Monterey, CA 93943.
E-mail: eahendri1@nps.edu

DOI: 10.1175/WAF-D-15-0016.1

(CMR) is well known to induce mesoscale circulations, which are quite challenging for numerical weather prediction models to capture (Fang and Kuo 2013). While the CMR is generally known to have relatively minor impacts on typhoon tracks, it can have dramatic effects on rainfall when the typhoon circulation interacts with the CMR (Wu et al. 2002).

Building on past work, here we will investigate how the model resolution and physics affect the simulation of Morakot, especially the quantitative precipitation forecast (QPF). Sensitivity tests on Typhoon Morakot (2009) are conducted using the U.S. Navy's Coupled Ocean–Atmosphere Mesoscale Prediction System–Tropical Cyclone (hereafter COAMPS-TC). The sensitivity tests span the horizontal resolution, cumulus parameterizations, and microphysical parameterizations, in which the precipitation forecast is expected to be most sensitive. In section 2, a brief synoptic history of Typhoon Morakot (2009) is presented. In section 3, the data and methods are described, including both the observations used for verification and the details of the numerical prediction model and setup. The results of the sensitivity tests are presented in section 4. A discussion of the results is given in section 5. The conclusions are given in section 6.

2. Synoptic history

Typhoon Morakot formed in the western North Pacific monsoon trough, approximately 1000 km to the east of the Philippines. It was identified as a tropical depression at 1800 UTC 3 August 2009 by the Joint Typhoon Warning Center (JTWC) and was subsequently classified as a tropical storm with maximum sustained winds of 35 kt (1 kt = 0.51 m s^{-1}) at 0600 UTC 4 August. Morakot tracked due westward and gradually intensified, making landfall on the eastern side of Taiwan at 1200 UTC 7 August as a minimum intensity typhoon with maximum sustained winds of 80 kt. Because of Morakot's large size, the minimum central pressure was quite low at this time for its maximum sustained winds: 963 hPa. After landfall, Morakot moved northwestward and slowed in translation speed. During this period, the storm interacted with the southwest monsoon and grew significantly in size. The cyclonic flow of Morakot in combination with the monsoon flow produced a stream of westerly-to-southwesterly flow in southwest Taiwan for an extended period of time (0000 UTC 8 August–0000 UTC 10 August). A band of extreme precipitation developed in a localized area along the southwest slopes of the CMR. This produced tremendous amounts of rainfall there (in excess of 2500 mm), leading to the disaster.

3. Data and methods

a. Observational data

The position and intensity of Typhoon Morakot were obtained from the JTWC best-track dataset. Intensity estimates were provided both in terms of 1-min maximum sustained surface wind and minimum central pressure. The observed precipitation was computed using a Barnes analysis on precipitation recorded from 381 rain gauge stations over Taiwan. A two-pass Barnes analysis was done, using a characteristic grid spacing of 7.5 km to compute the weights associated with each rain gauge observation. Prior to the analysis, the precipitation was accumulated in each rain gauge for the 3-day period: 1200 UTC 6 August–1200 UTC 9 August. The Barnes analyses was performed on a 0.025° × 0.025° latitude–longitude grid (approximately 3-km horizontal resolution) from 21.5° to 25.5°N and 120° to 122°E. For qualitative comparisons of the structure, the land-based radar data composites provided by Taiwan's Central Weather Bureau (CWB) were used.

b. Model description

The mesoscale model used here is a special version of COAMPS-TC. A description of the original COAMPS model[1] is given in Hodur (1997) and more details can also be found in Chen et al. (2003). The model uses a terrain-following sigma-height coordinate and the nonhydrostatic compressible equations of motion (Klemp and Wilhelmson 1978). The microphysical parameterization is based on the work of Rutledge and Hobbs (1983) and Lin et al. (1983), with prognostic equations for mixing ratios of cloud droplets, ice particles, rain, snow, graupel, and drizzle. The model also includes a shortwave and longwave radiation parameterization (Fu and Liou 1993), as well as a planetary boundary layer parameterization with a 1.5-order turbulence closure (Mellor and Yamada 1982).

The tropical cyclone prediction version COAMPS-TC (Doyle et al. 2011, 2014) includes the following enhancements: (i) synthetic wind and mass observations of the TC based on the operational warning message (Liou and Sashegyi 2011), (ii) relocation of the first-guess field to the observed TC position, (iii) TC-following nested inner grids using an automatic TC tracker (not used for these tests), (iv) dissipative heating (Jin et al. 2007), and (v) a surface drag coefficient that approaches 2.5 × 10^{-3} for wind speeds exceeding 35 m s^{-1} (Donelan et al.

[1] COAMPS is a registered trademark of the Naval Research Laboratory.

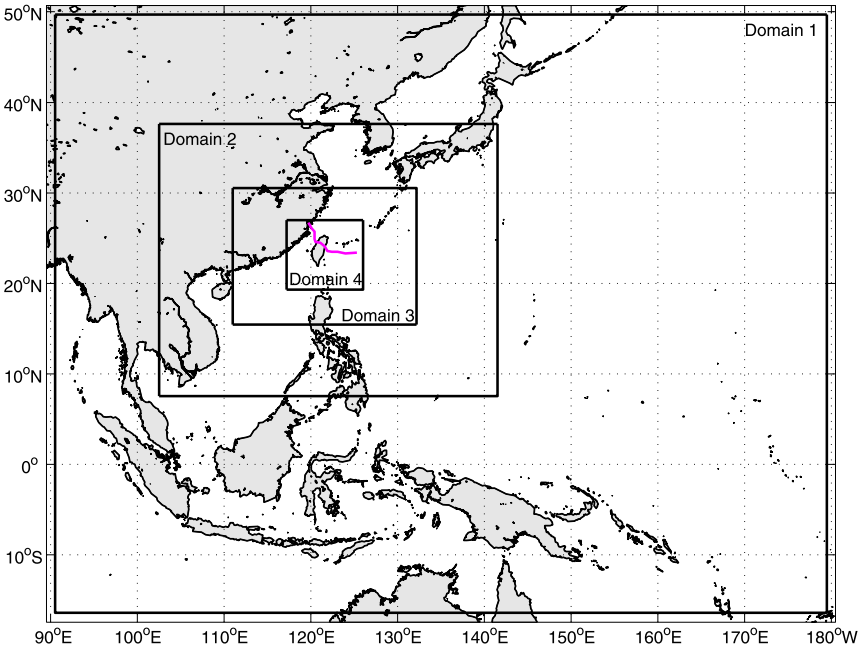

FIG. 1. The nested domains used for the sensitivity tests. CNTL, SAS2, SAS3, and THOMP use domains 1–3 with a finest resolution of 5 km. COARSE uses only domains 1 and 2, and FINE uses domains 1–4. All domains remain fixed in space during the model simulation. The JTWC best track of Morakot from 1200 UTC 6 Aug to 1200 UTC 9 Aug is given in purple.

2004). The forecast system also has a capability for ocean coupling; however, for this study the model was run in stand-alone atmosphere mode. COAMPS-TC is currently an operational model for the U.S. Navy and is run in real time in every ocean basin. The model setup for these experiments differs from the operational model runs in that fixed (instead of moving) nests are used and the initialization scheme is different.

c. *Model setup and sensitivity tests*

A control simulation and a number of sensitivity tests were conducted. The sensitivity tests include different horizontal grid spacings, cumulus parameterizations, and microphysical parameterizations. The domain setup for all tests is shown in Fig. 1. The sensitivity tests use various configurations of these domains, which are described below. The entire track of Morakot from 1200 UTC 6 August to 1200 UTC 9 August is contained in domain 4 in Fig. 1.

The list of the sensitivity tests is given in Table 1. The control simulation (CNTL) uses three fixed domains (domains 1–3) in Fig. 1, with resolutions of 45, 15, and 5 km on domains 1, 2, and 3, respectively. Two-way interactive nesting is applied for all nested domains. The Kain–Fritsch parameterization (KF; Kain 2004; Kain and Fritsch 1993, 1990) was used on domains 1 and 2 to help resolve the effects of subgrid-scale convection, while the microphysical parameterization was active on all domains. The SAS2 simulation is exactly the same as CNTL, except the simplified Arakawa–Schubert parameterization (SAS; Han and Pan 2011; Pan and Wu 1995) was used in place of the Kain–Fritsch parameterization on the outer two domains. In the SAS3 simulation, the SAS parameterization is used on all three domains, since 5 km could be construed as being a little too coarse to explicitly resolve convection using microphysics only. The SAS and KF schemes represent two widely used convection parameterizations for numerical weather prediction. The SAS scheme retains from the classic Arakawa–Schubert (AS; Arakawa and Schubert 1974) parameterization a closure relation based on an adjustment toward an assumed climatological relationship between ''cloud work function'' and cloud-top height. The cloud work function is essentially the level-by-level updraft mass-flux-weighted convective available potential energy (CAPE). The SAS scheme simplifies the AS formulation in allowing for only one cloud-top height at a given model time step, thus avoiding a costly computation of intercloud-type interactions. The KF scheme differs from the SAS scheme in some important aspects, making it a good choice for the comparisons examined in this work. One of the key features of interest in the KF scheme is its ''convective triggering'' parameterization, which, in contrast to the SAS treatment, attempts to represent the effect of subgrid-scale updraft temperature perturbations in determining when convection can be expected to occur.

TABLE 1. Descriptions of numerical simulations.

Test name	Resolution (km)	Description
CNTL	5	Control expt
SAS2	5	SAS across domains 1 and 2, explicit convection on domain 3
SAS3	5	SAS across all three domains
THOMP	5	Thompson microphysics across all domains
COARSE	15	Same as CNTL, but only using domains 1 and 2
FINE	1.67	Same as CNTL, but with domain 4

Another distinctive feature of the KF scheme is its ''buoyancy sorting'' parameterization of updraft-environment mixing. Although the SAS scheme includes an imposed reduction of updraft mass flux in dry environments, the buoyancy-sorting treatment in the KF scheme potentially allows the updraft mass flux to respond more realistically to changes in both atmospheric humidity and parcel buoyancy, based on computed buoyancies of an ensemble of mixed subparcels of updraft and environmental air.

With regard to the microphysics, the THOMP simulation is the same as the CNTL run, except the Thompson microphysics scheme (Thompson et al. 2008) is used instead of the COAMPS microphysical parameterization. The COAMPS microphysical scheme used in the CNTL simulation is a relatively typical single-moment scheme with five hydrometeor species: cloud water and ice, rain, snow, and graupel. This scheme is derived from Rutledge and Hobbs (1983), which is similar to the Lin et al. (1983) treatment. The Thompson microphysics scheme (Thompson et al. 2008) uses a hybrid double-moment approach in cloud ice and rain and a single-moment approach in the other three species. The upper-level cloud ice concentrations produced by the COAMPS scheme are up to two orders of magnitude greater than those of the Thompson scheme, primarily because of the differing assumptions concerning the ice nucleation parameterization. Other noteworthy differences between the Thompson and COAMPS schemes include the ice crystal terminal velocity and the threshold at which the cloud ice is converted into snow. These differences have been summarized in Table 3 in Jin et al. (2014). Additionally, the Thompson scheme incorporates recent findings from numerous field campaigns in an effort to reduce what has been noted by previous studies as a high bias in precipitation efficiency (Colle et al. 1999). As stated above, the Thompson scheme has significant differences in the treatment of ice and snow, and its impact has been systematically evaluated in COAMPS-TC for TC track and intensity forecasts (Jin et al. 2014). However, the Thompson scheme has not been examined for TC precipitation forecasts, and therefore it is interesting to examine it here in comparison to the COAMPS microphysical parameterization.

The COARSE simulation is the same as the CNTL run, except the 5-km domain is not used (only the 15- and 45-km domains are used). Finally, the FINE simulation is identical to the CNTL simulation, except the fourth domain with a horizontal grid spacing of 1.67 km is used additionally (Fig. 1). The Taiwanese terrain corresponding to the 15-, 5-, and 1.67-km meshes is shown in Fig. 2. The 15-km domain resolves some of the broad features of the topography, the 5-km domain is able to represent more detail and higher peaks, and the 1.67-km domain further resolves many finescale features. While the 15-km domain is obviously not expected to yield as good a precipitation forecast as the 5- and 1.67-km domains because of its inability to accurately resolve the terrain interaction, it is included to understand the effects of varying resolution on the precipitation forecast.

For all tests, the model was run with 40 sigma levels in the vertical with a model top at 31 km (recall, COAMPS-TC uses a sigma-height vertical coordinate rather than sigma pressure). The first forecast of Morakot was initialized at 0000 UTC 6 August, using the global analysis from the Navy Operational Global Atmospheric Prediction System (NOGAPS; Hogan and Rosmond 1991) as the first guess. The NOGAPS analysis here is at a horizontal resolution of 1° latitude × 1° longitude (or approximately 100 km). Subsequently, two forecasts using the previous 6-h COAMPS-TC forecasts as a first guess in the data assimilation were executed at 0600 and 1200 UTC 6 August, identified here as warm starts. For each analysis, the Naval Research Laboratory Atmospheric Variational Data Assimilation System (NAVDAS; Daley and Barker 2001) was used to optimally blend all observations (including the TC synthetic observations) with the first guess to create the analysis. The 72-h forecast beginning at 1200 UTC 6 August was used for all verifications. This forecast initial time was approximately 24 h before landfall and encompasses the time period when most of the precipitation was recorded in Taiwan.

4. Sensitivity tests

a. Track and intensity

The tracks of all of the sensitivity tests are given in Fig. 3a and the intensity is given in Figs. 3b and 3c, by 1-min maximum sustained wind and minimum central pressure, respectively. In all panels, the solid black line is the JTWC best track, and the colored curves are the COAMPS-TC forecasts from the different sensitivity tests.

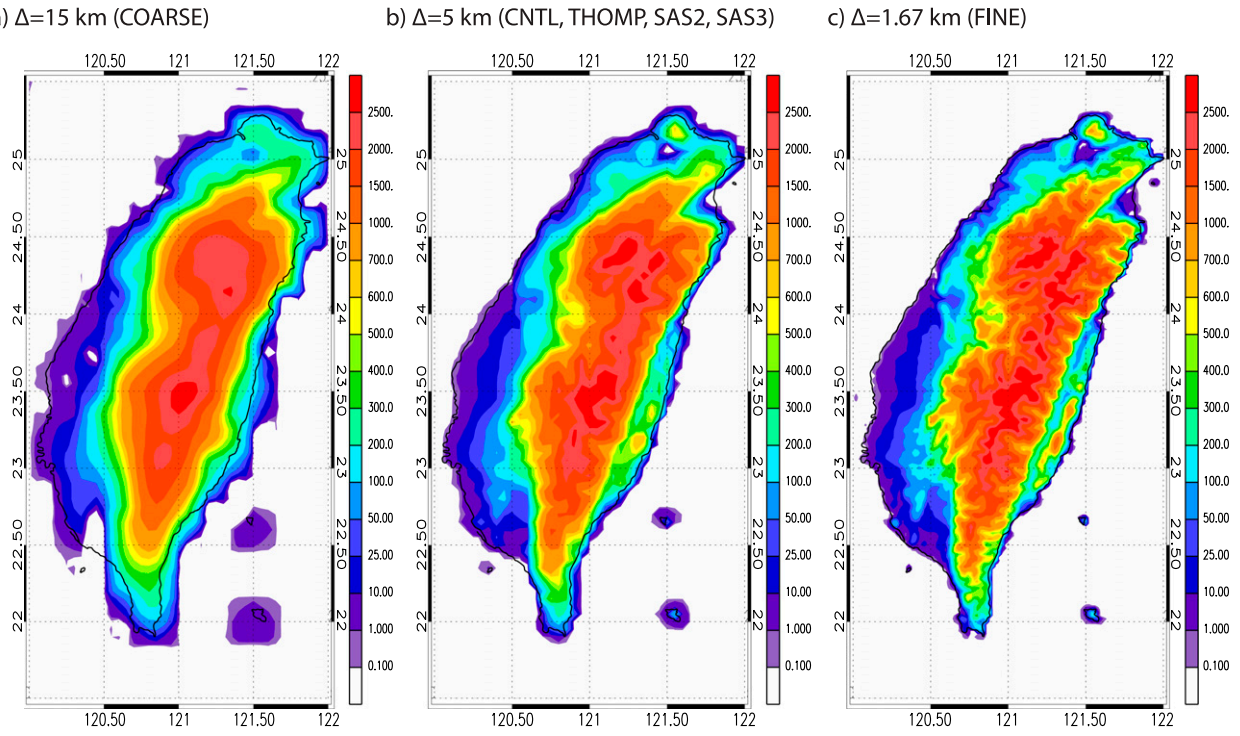

FIG. 2. Taiwan terrain (m) in COAMPS-TC at different horizontal grid spacings: (a) 15, (b) 5, and (c) 1.67 km.

Examining Fig. 3a, the center of the observed Morakot moved over north-central Taiwan, and then moved northwest over the Taiwan Strait into southeast China. Note that Morakot had a large circulation pattern, and its effects extended far from its center, particularly after its first landfall. The tracks of the different sensitivity tests exhibit some variability about the observed track, but most tests are close to the observed track. The CNTL, THOMP, FINE, and COARSE simulations take Morakot over Taiwan and to the northwest into China. The SAS3 and SAS2 simulations move Morakot north too early. The results indicate that the track is relatively insensitive to varying the horizontal resolution and microphysics, but it is sensitive to varying the cumulus parameterization. Examining the intensity in Figs. 3b and 3c, the CNTL, THOMP, and FINE runs are in closer agreement with the JTWC best track than are the SAS2, SAS3, and COARSE runs. The variance in initial intensity between the simulations is a result of using the warm update cycle described above in conjunction with data assimilation with synthetic observations. Differences in the background first-guess field between each experiment can lead to slight differences in the initial intensity and position. While there may be some sensitivity of the results to the variability in the initial conditions, model physics tend to be more important for the track, intensity, and precipitation in the longer term (after $t = 24$ h), which is the focus of this study.

Further analysis of the track and intensity errors versus lead time is given in Fig. 4. The track error is calculated using the Haversine formula for the distance between two points on a sphere. The intensity error is calculated as the absolute value of the difference between the JTWC best-track intensity and the simulated maximum intensity. Examining the track errors, the CNTL and THOMP simulations have the best track errors overall. The FINE and COARSE simulations have slightly worse overall errors, and the SAS2 and SAS3 simulations have the largest errors, particularly at later lead times from recurving Morakot too far north. With regard to intensity, the CNTL, THOMP, and FINE simulations all have low absolute intensity errors in terms of sea level pressure and maximum sustained wind. The COARSE simulation has a larger intensity error at the early lead times, as the resolution is too coarse to resolve the vortex. The SAS2 and SAS3 simulations have larger intensity errors at the later lead times, as they keep Morakot too strong because it is not interacting with land.

In Fig. 5, the 500-hPa geopotential height and winds are shown for the CNTL and SAS2 simulations on domain 2 at $t = 48$ h. In Figs. 5a and 5b, the 500-hPa geopotential height is shown for the CNTL and SAS2 simulations, respectively; in Figs. 5c and 5d, the 700-hPa velocity vector magnitude and vectors are shown; and in Figs. 5e and 5f, the 850-hPa velocity vector magnitude

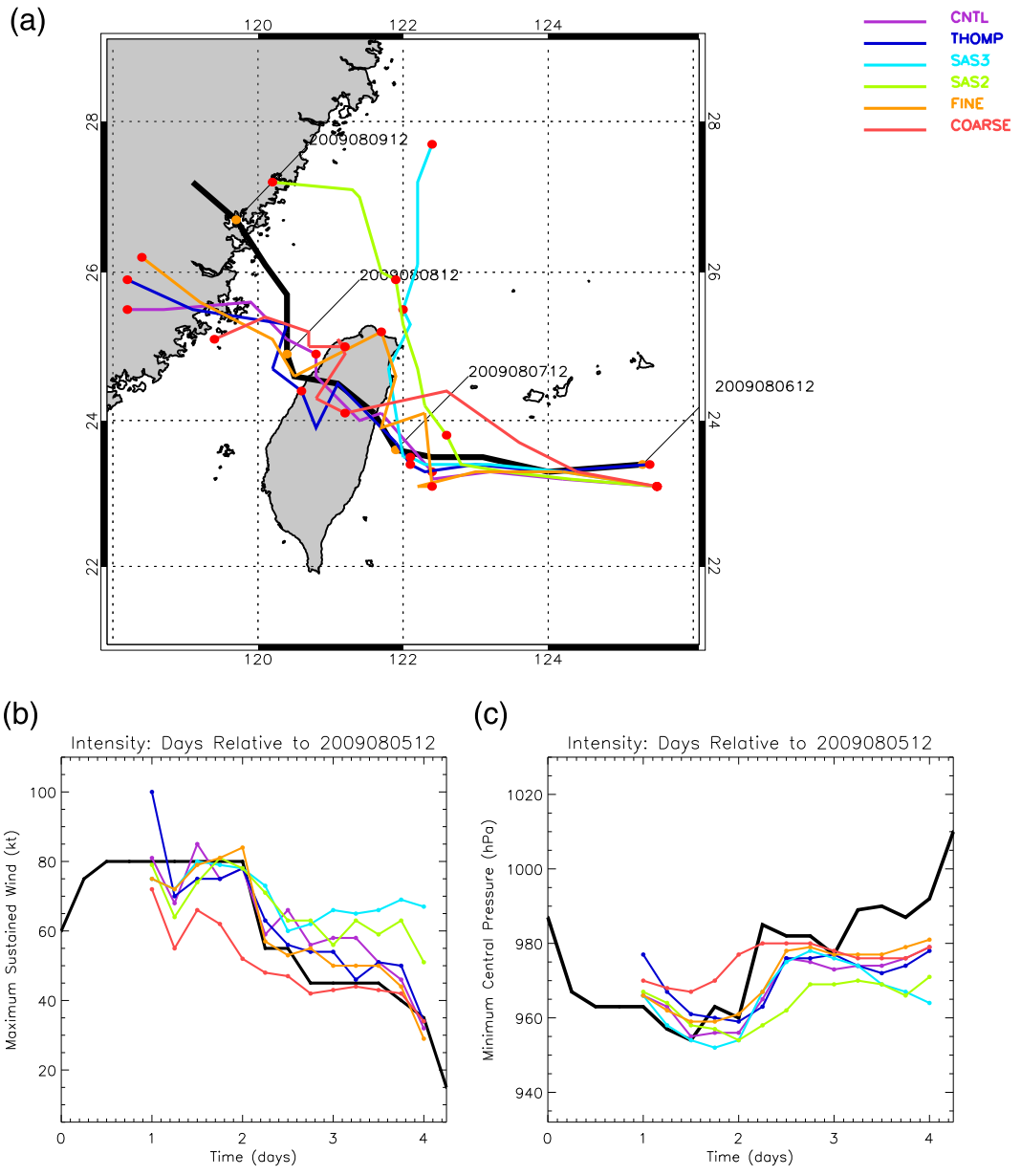

FIG. 3. Track and intensity verification for all sensitivity tests: (a) tracks, (b) maximum sustained wind (kt), and (c) minimum central pressure (hPa). The black curve is the JTWC best track and colored curves are the sensitivity tests with COAMPS-TC. In the track plots, the solid circles denote the position at 24-h intervals.

and vectors are shown. Significant differences are evident between the CNTL and SAS2 simulations with regard to the environment near Morakot. In the SAS2 simulation, a separate coherent vortex is apparent to the southwest of Morakot, while in the CNTL simulation an extended trough exists. The vortex in the SAS2 simulation is a result of the regeneration of the remnants of Tropical Storm Goni, which existed while Morakot was farther east from Taiwan. The erroneous regeneration of Goni caused significant large-scale steering flow differences in the SAS2 experiment. In particular, there exists a second southwesterly wind maximum associated with Goni in both the 850- and 500-hPa wind plots, causing a much stronger and larger region of southwesterly flow, which helped move Morakot farther north. This regeneration did not occur in reality, but rather Goni decayed into an extended surface trough to the southwest of Morakot (similar to the CNTL simulation) (Wu 2013; Hendricks et al. 2011). To demonstrate this quantitatively, the steering flow at $t = 48$ h is

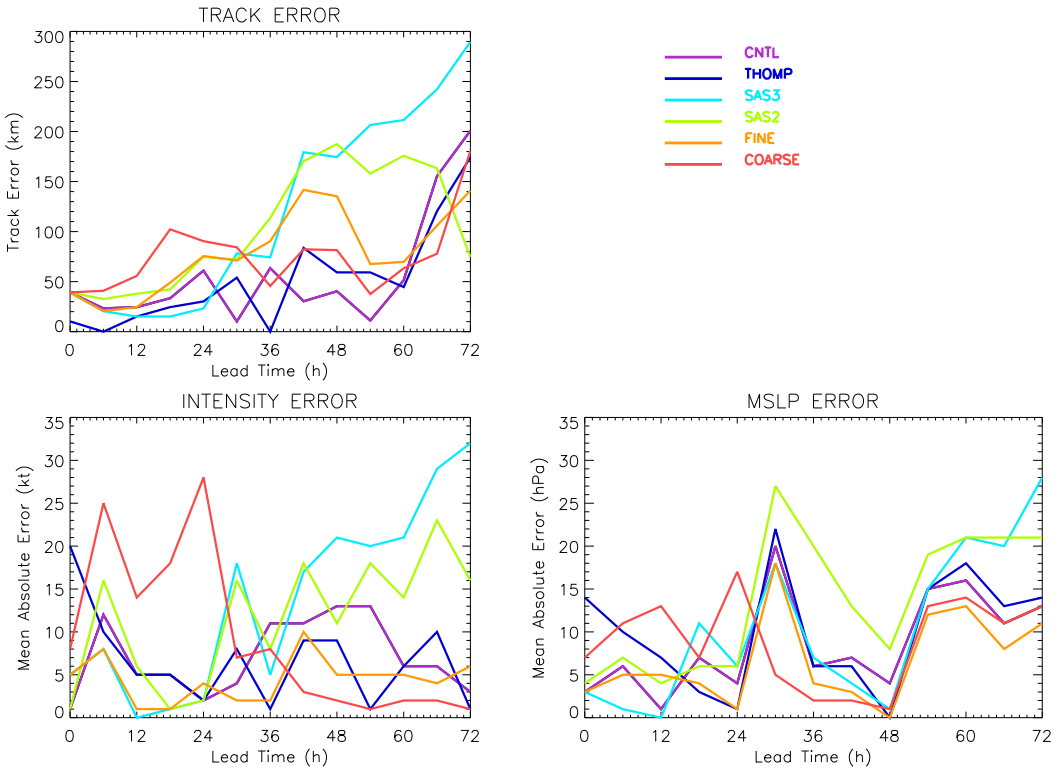

FIG. 4. Track and intensity errors as a function of lead time for all the sensitivity tests. Errors are calculated with respect to the JTWC best track data.

shown for each experiment in Table 2, consistent with the methods described in Chan and Gray (1982) and Evans et al. (1991). Additionally, the steering flow calculated from the National Centers for Environmental Prediction (NCEP) final (FNL) operational analysis is given as a proxy for the observed steering flow. For each simulation and the NCEP FNL analysis, the average 850–500-hPa zonal and meridional components of the velocity are shown in a 1000-km box centered on Morakot. Both the SAS2 and SAS3 runs have significantly larger average meridional velocity components (3.42 and 3.38 m s^{-1}, respectively) than the other runs and the FNL analysis (2.71 m s^{-1}). In summary, the erroneous regeneration of Goni (as well as another cyclone to its east) in the SAS simulations modified the large-scale flow in which Morakot was embedded, causing a more southerly component to the steering flow.

All of the simulations do a reasonable job of predicting the gradual weakening of Morakot as it interacted with the CMR of Taiwan. With regard to horizontal resolution, the COARSE simulation performed the worst. This is expected since 15-km resolution is generally known to be incapable of resolving the inner core and the features responsible for intensity variability, as well as the typhoon–terrain interaction. The CNTL simulation at 5-km resolution performed reasonably well, and the FINE simulation at 1.67-km performed the best out of all the sensitivity tests. This simulation was able to capture the sharp weakening at landfall, and gradual weakening thereafter. Both the CNTL and THOMP simulations performed well in terms of intensity. The SAS2 and SAS3 simulations had larger errors in intensity as a result of the erroneous tracks for these cases. In summary, the track prediction accuracy is critical in determining the intensity error when the system is near complex terrain and interacting with large-scale environmental features.

b. *Structure*

To understand the precipitation forecast for each simulation, the simulated radar reflectivity is given in Figs. 6, 7, and 8 in comparison to the Taiwan CWB radar composite. The structure is shown near the landfall time (1200 UTC 7 August) in Fig. 6. In Fig. 7 the structure is shown after landfall (1200 UTC 8 August). In Fig. 8 (0000 UTC 9 August), the structure is shown as Morakot grew in size and was interacting with the southwest monsoon, producing consistent upslope flow on the western side of the southern CMR. The simulated radar reflectivity algorithm is based upon Rutledge and Hobbs (1983).

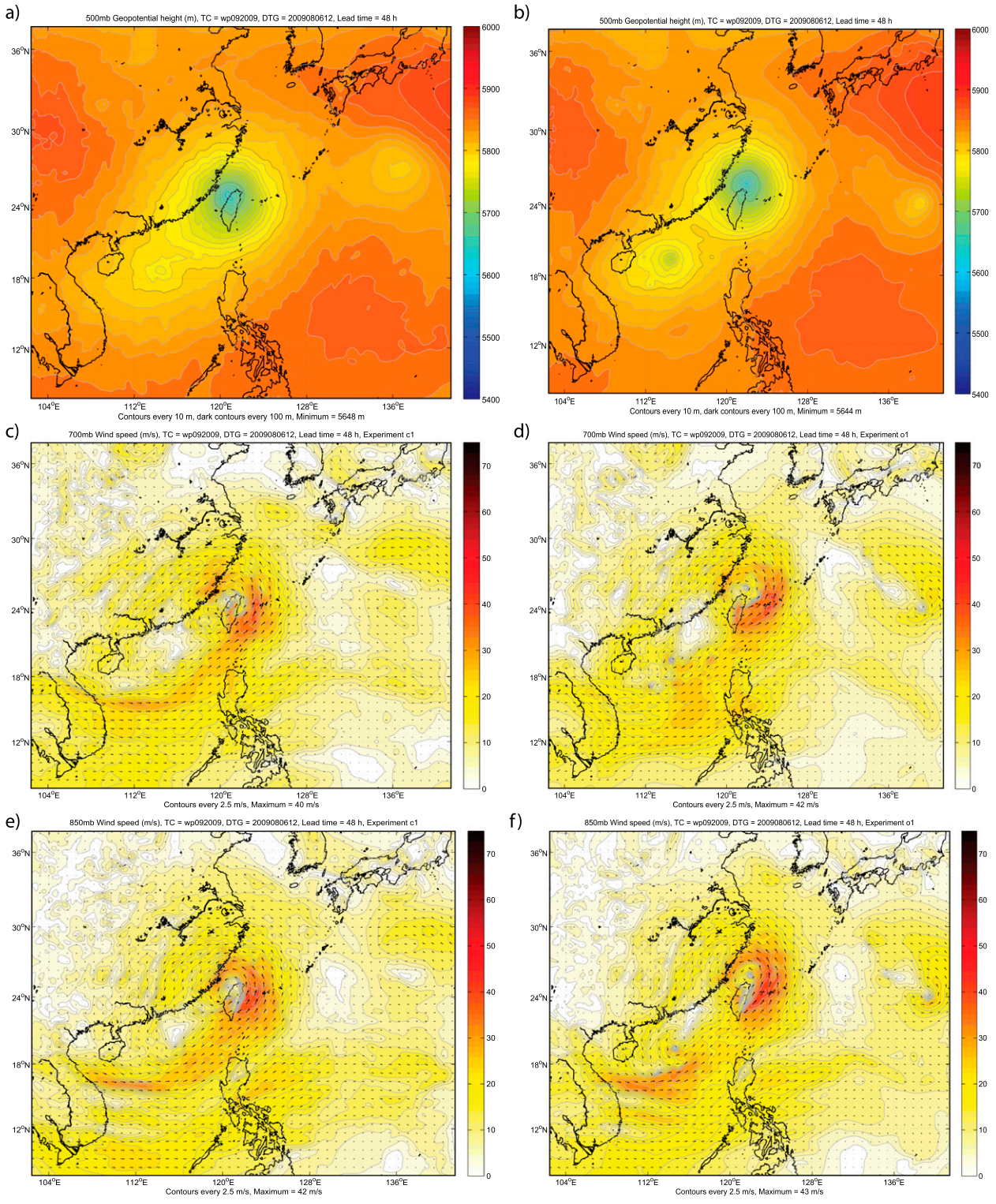

FIG. 5. Comparisons of the large-scale flow pattern between the CNTL and SAS2 experiments on domain 2 at $t = 48$ h (valid at 1200 UTC 8 Aug 2009). The 500-hPa geopotential height for the (a) CNTL and (b) SAS2 experiments; the 700-hPa wind speed and vectors for the (c) CNTL and (d) SAS2 experiments; and the 850-hPa wind speed and vectors for the (e) CNTL and (f) SAS 2 experiments.

TABLE 2. Average steering flow vector components (850–500 hPa) around Morakot at $t = 48$ h. Data are from an approximate 1000-km box centered on Morakot (21°–31°N, 115°–125°E) at this time. Each simulation is listed along with the calculations from the NCEP FNL analysis.

Test name	Avg zonal velocity ($m\,s^{-1}$)	Avg meridional velocity ($m\,s^{-1}$)
CNTL	−1.25	2.50
SAS2	−1.45	3.42
SAS3	−1.63	3.38
THOMP	−2.09	1.75
COARSE	−1.29	2.70
FINE	−1.56	2.73
FNL	−0.18	2.71

Examining Fig. 6, prior to landfall, all the simulations depict the higher reflectivity to the south of the center, similar to the CWB radar composite. Overall, the THOMP simulation has higher reflectivities than were observed. The sensitivity to the resolution is evident by comparing the CNTL, COARSE, and FINE simulations, with the broad region of precipitation captured by all simulations, and more detailed convective structure evident in the FINE simulation. The SAS3 simulation exhibits smoother reflectivity with more banding, while SAS2 is more similar to the CNTL on grid 3, as expected. In Fig. 7 (after landfall), the CNTL simulation compares well with the CWB radar composite, capturing the southwest–northeast-oriented band of moderate precipitation as well as the precipitation directly southwest of the center. While the THOMP simulation has higher reflectivities than the CWB radar composite at this time as well, the band of vigorous convection to the south (with its midsection located near the southern tip of Taiwan) closely matches the CWB radar composite. The FINE simulation also compares reasonably well with the observations in capturing the large southwest–northeast-oriented band, but does not capture the precipitation directly south of the center as well as the CNTL simulation. The outer band of convection is located too far south compared to the CNTL simulation. Both the SAS2 and SAS3 simulations bring the center of Morakot too far north and, thus, have significant position errors in the southwest–northeast-oriented band. As discussed earlier, this is due to the erroneous amplification of the remnants of Goni, which perturbed the large-scale steering flow of Morakot. Finally, in Fig. 8, the comparison is shown at 0000 UTC 9 August. Here, the orientation of the southern band in the CNTL simulation is significantly different than the CWB composite (oriented more south–north, rather than southwest–northeast). The FINE simulation has this band displaced too far south in comparison to the CWB composite. The SAS2 and SAS3 simulations here also have Morakot being too symmetric and too far north.

c. Precipitation

The 3-day accumulated precipitation (from 1200 UTC 6 August to 1200 9 August) for each simulation in comparison to the Barnes analysis of the Taiwan rain gauge measurements is given in Fig. 9. For this comparison, the model forecast fields were interpolated onto the same grid as the Barnes analysis. In the observation analysis, the locations of all of the rain gauges in Taiwan are shown as black dots. Note that there are many more stations on the western side of the CMR than on the eastern side and on the CMR peaks. The analysis shows extremely large precipitation amounts (in excess of 1500 mm) over a large region of the southern CMR.

All simulations produce a precipitation maximum in southern Taiwan, which is qualitatively similar to the observational analysis. Of these simulations, the CNTL and THOMP agree the best with the observations, also capturing the secondary peak in the northern CMR. The SAS2 and SAS3 simulations capture the southern maximum but also have too much precipitation in the northern CMR in comparison to the observational analysis. This occurred because the tracks of the SAS2 and SAS3 simulations deviated too far north in comparison to the actual track. With regard to varying grid resolution, the CNTL simulation at 5 km has the best qualitative agreement with the observations. The COARSE simulation produces too little precipitation because it is not convective permitting, it is too coarse to resolve the interaction of the typhoon circulation with the orography, and the intensity is too weak (Fig. 3). Surprisingly, the FINE simulation shows less qualitative agreement with the observations than does the CNTL simulation. It is able to capture the extreme precipitation over the peaks of the southern CMR, but produces too little precipitation over the southwest portion of Taiwan. This is partly due to the southwest–northeast-oriented precipitation band being displaced too far south at 0000 UTC 9 August. Moreover in the northern CMR, there is too little precipitation as well. By varying the microphysics from the COAMPS scheme to the Thompson scheme, larger precipitation amounts were found in southwest Taiwan, exceeding the observations. To further understand the differences between the CNTL and THOMP experiments, Fig. 10 compares the hydrometeor distributions along the CMR at the 6-h forecast lead time (1800 UTC 6 August). At this time, still early into the simulation, the simulated storm is more than 400 km away, to the east of Taiwan (Fig. 3a), and there is similar intensity when

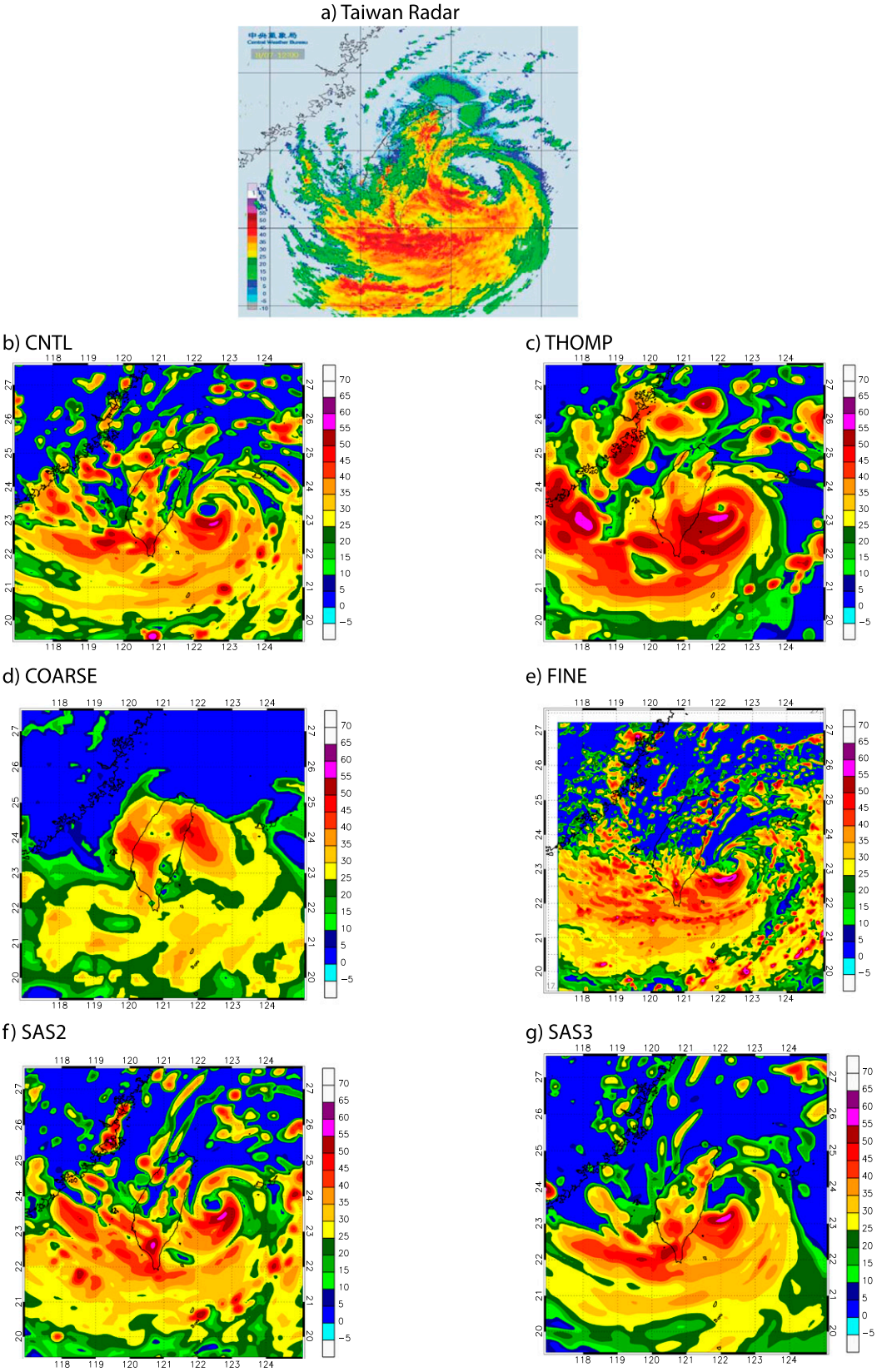

FIG. 6. Comparison of the CWB radar composite with the simulated radar reflectivity (dBZ) at $t = 24$ h (valid at 1200 UTC 7 Aug) for all the experiments. (a) Taiwan CWB radar composite, and the (b) CNTL, (c) THOMP, (d) COARSE, (e) FINE, (f) SAS2, and (g) SAS3 simulations.

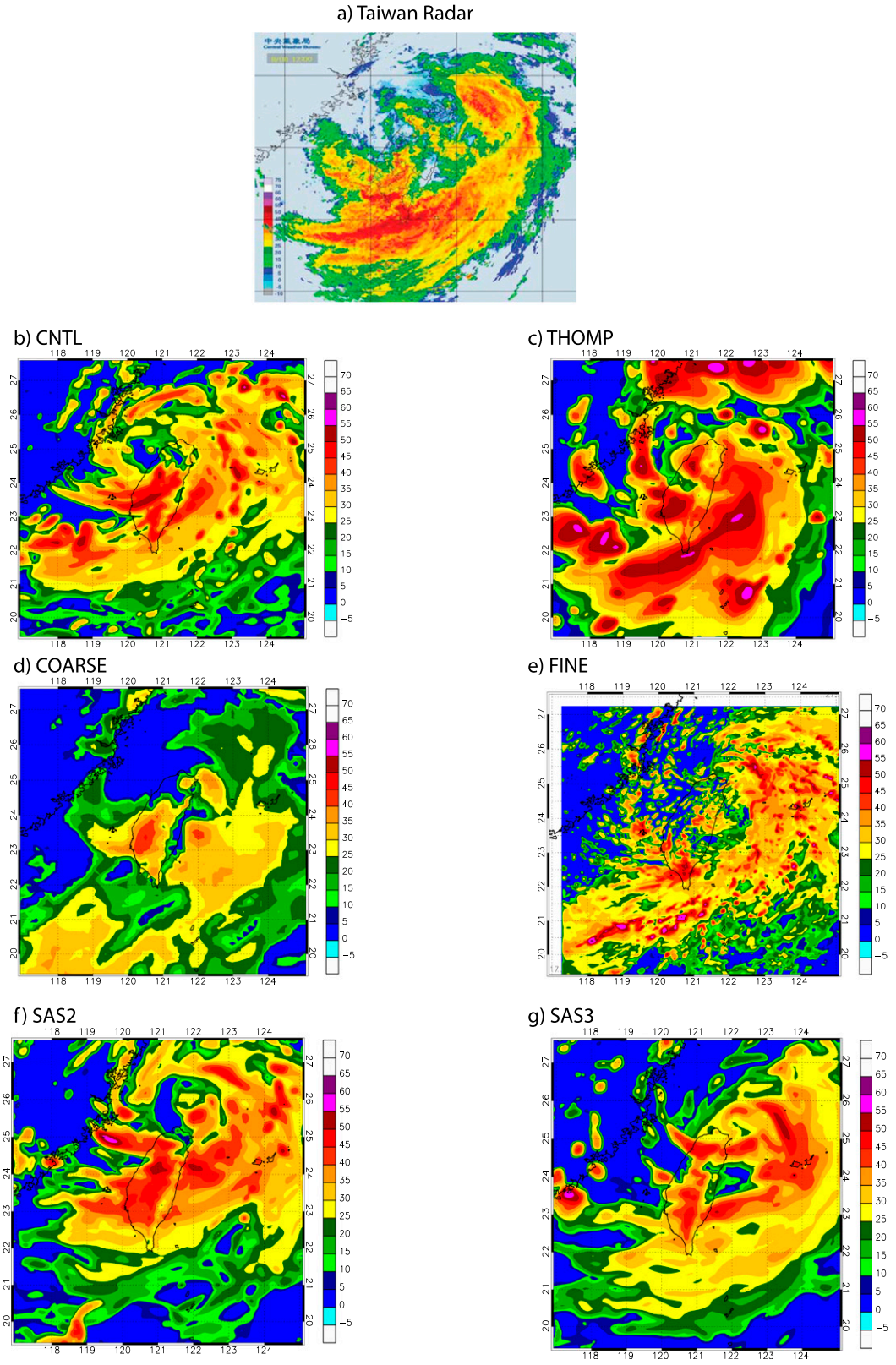

FIG. 7. As in Fig. 6, but at $t = 48$ h (valid at 1200 UTC 8 Aug).

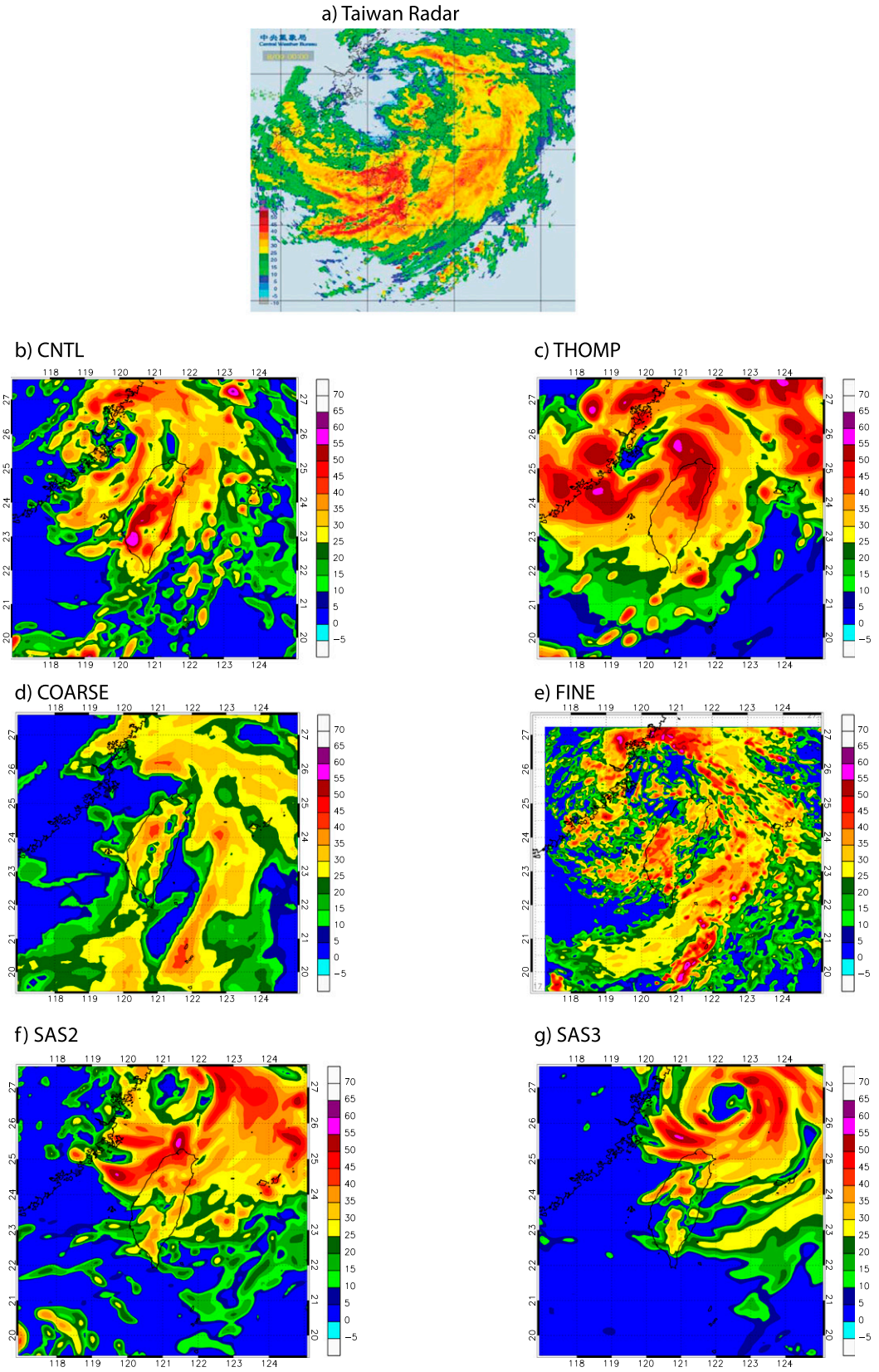

FIG. 8. As in Fig. 6, but at $t = 60$ h (valid at 0000 UTC 9 Aug).

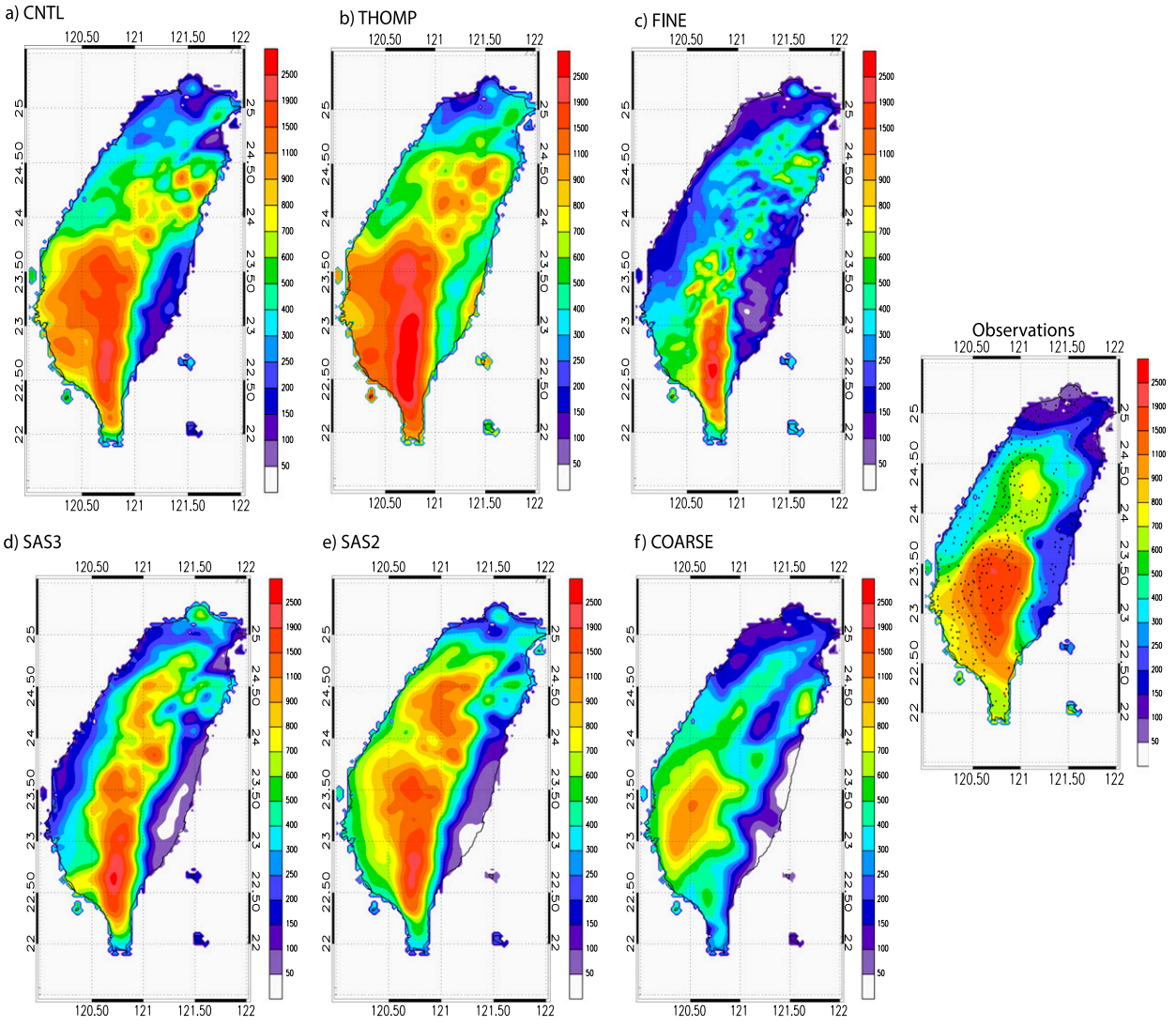

FIG. 9. The 3-day accumulated precipitation amounts (mm) from 1200 UTC 6 Aug through 1200 UTC 9 Aug.

comparing CNTL and THOMP. However, significant differences exist in the hydrometeor distribution. The Thompson microphysical scheme produced much higher snow mixing ratios (exceeding 3 g kg^{-1} over the northern edge of the cross section) compared to 0.4 g kg^{-1} produced by the CNTL. The rain mixing ratio increases as the snow falls into the warmer layers and results in more rainfall in THOMP. Furthermore, the snow particles in the THOMP experiment extended southward, and more rain is expected over the CMR as the snow falls from the anvil clouds. On the other hand, the CNTL test produced more ice particles (up to two orders of magnitude more) than THOMP.

Further analysis of the QPFs was conducted using the equitable threat score (ETS), the threat score (TS), and the bias score (BS). The ETS, TS, and BS are defined as

$$\mathrm{ETS} = \frac{H - R}{O + F - H - R}, \tag{1}$$

$$\mathrm{TS} = \frac{H}{O + F - H}, \quad \text{and} \tag{2}$$

$$\mathrm{BS} = \frac{F}{O}, \tag{3}$$

where O is the number of points where the observed rainfall exceeds a threshold, F is the number of points where the model-predicted rainfall exceeds a threshold, H is the hit area (the intersection of O and F points), and $R = FO/N$ is the expected number of points of F to fall inside O by chance (or the random hit area), where N is the total number of observations. These scores have been

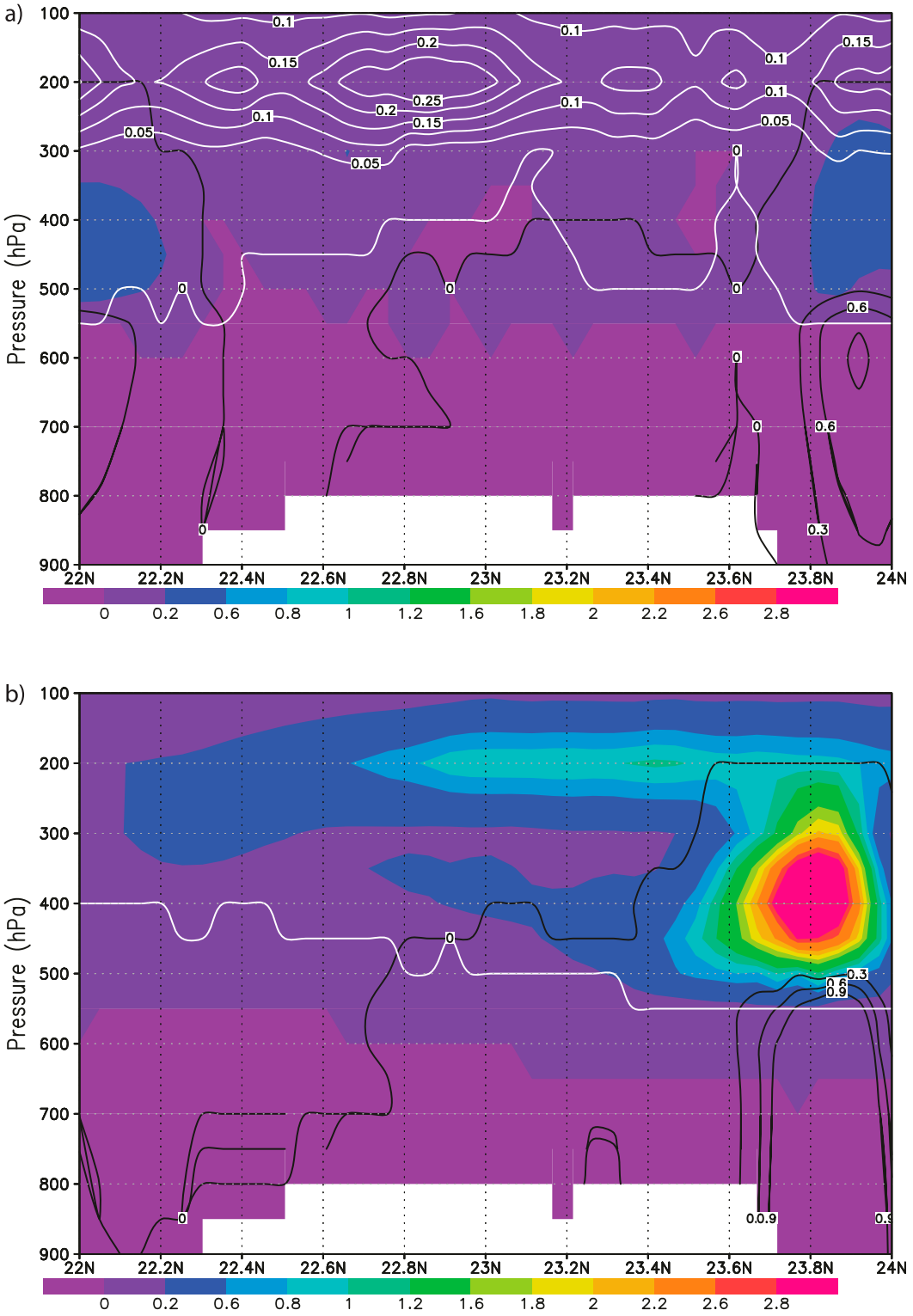

FIG. 10. Vertical cross sections of hydrometeors along 120.8°E from 22° to 24°N from 900 to 100 hPa for the (a) CNTL and (b) THOMP tests at $t = 6$ h, showing snow mixing ratio (g kg^{-1}, shaded), rain mixing ratio (black contours at 0.3 g kg^{-1} intervals), and cloud ice mixing ratio (white contours at 0.05 g kg^{-1} intervals). The cloud ice mixing ratio from THOMP is about two orders of magnitude smaller than that from CNTL; hence, it is not shown with 0.05 contour intervals as in (a).

TABLE 3. QPF verification scores. The ETS, TS, and BS as computed by the Barnes analysis method for the observed precipitation (denoted by B) and by directly comparing the model data at the precipitation station locations (denoted by S).

	ETS-B	TS-B	BS-B	ETS-S	TS-S	BS-S
500-mm threshold						
CNTL	0.49	0.73	1.11	0.56	0.74	1.12
SAS2	0.31	0.62	1.22	0.38	0.64	1.25
SAS3	0.42	0.63	0.82	0.49	0.68	0.89
THOMP	0.31	0.65	1.51	0.45	0.71	1.40
COARSE	0.25	0.46	0.62	0.27	0.46	0.65
FINE	0.24	0.40	0.45	0.22	0.36	0.41
1000-mm threshold						
CNTL	0.51	0.58	1.29	0.50	0.57	1.34
SAS2	0.42	0.50	1.14	0.40	0.48	1.16
SAS3	0.37	0.43	0.68	0.28	0.33	0.49
THOMP	0.34	0.45	2.01	0.37	0.47	1.95
COARSE	0.11	0.14	0.16	0.08	0.09	0.09
FINE	0.17	0.22	0.31	0.06	0.07	0.10

used extensively for QPF verification (see Wang 2014 and references therein).

Two precipitation thresholds were used to calculate the scores (500 and 1000 mm). These are very high values because of the extreme precipitation observed during Morakot. It is our goal to understand which model configurations can be used to capture the extreme precipitation associated with Morakot, and not necessarily the weaker amounts. Since to first order, the track of the TC is the largest factor in the QPF errors, the scores are plotted versus the average track error for all lead times. The QPF scores were calculated using two different methods. In the first method, the scores are computed using the observational Barnes analysis and COAMPS-TC forecasts interpolated onto the regular grid described in section 3a. In the second method, the COAMPS-TC forecasts were interpolated directly to the rain gauge station location. Both of these scores are shown in Table 3. Minor differences are evident in the scores by using the different methods. The QPF scores using the second method are also plotted versus the average track error in Fig. 11. The average track error is defined as the average of all track errors from $t = 0$ to 72 h, at 6-h intervals (Fig. 4).

Generally speaking, an inverse relationship would be expected between the ETS/TS and average track error if a tropical cyclone were purely symmetric and terrain effects were neglected. This inverse relationship is broadly evident between the THOMP, CNTL, COARSE, and FINE simulations. In Figs. 11a and 11b, it can be seen that the CNTL simulation has the highest ETS at both thresholds (500 and 1000 mm). The COARSE and FINE simulations had a lower ETS and slightly higher track errors. While the slightly worse track errors likely contributed to the QPF errors in both of these cases, other factors discussed previously were important as well. The COARSE run is not of high enough resolution to produce a strong enough typhoon circulation nor resolve the typhoon–terrain interaction. The FINE run had a position error of the southwest–northeast-oriented band of precipitation being to the south of Morakot's center. Additionally, the smoothing that is implicit in the Barnes analysis may have contributed to poorer performance scores for the FINE run. The SAS2 and SAS3 simulations actually had a higher ETS relative to the COARSE and FINE simulations, even though the track error was worse. The TS is given at both thresholds in Figs. 11c and 11d. Again, here the CNTL has the highest TS and a low average track error. A similar picture exists with the ETS in that the SAS and THOMP simulations have a higher TS, and both the COARSE and FINE simulations have a lower TS. The BS is given in Figs. 11e and 11f. A BS value of 1.0 is perfect, BS < 1 indicates an underprediction in precipitation, and BS > 1 indicates an overprediction in precipitation. At both thresholds, the COARSE and FINE simulations tend to underpredict the total areas of extreme precipitation. The CNTL simulation slightly overpredicts the precipitation, while the THOMP simulation has a significant overprediction of the precipitation amounts. The SAS2 simulation slightly overpredicts the precipitation, while the SAS3 simulation slightly underpredicts the precipitation. In summary, the QPF scores confirm the qualitative comparison in Fig. 8, demonstrating that the CNTL simulation has the best performance overall. The good performance is due to both the accurate track forecast and structure forecasts shown in Figs. 6–8.

Figure 12 shows a scatterplot of the model-predicted versus observed accumulated precipitation at each Taiwan rain gauge from 1200 UTC 6 August to 1200 UTC 9 August 2009 for each experiment. The abscissa is the measured accumulated precipitation, and the ordinate is the simulated accumulated precipitation. The perfect correlation is shown as a dashed line, and the factor of 2 regime is bounded by the dotted lines. The CNTL simulation has the best overall correlation, with most stations predicted within a factor of 2 and no significant bias. The THOMP scheme (Fig. 12b) exhibits similar scatter; however, the model overprediction bias is evident. The SAS2 and SAS3 schemes exhibit more scatter, partly because of the poorer tracks of these experiments. The COARSE simulation exhibits similar scatter as the SAS simulations. The FINE simulation exhibits less scatter; however, the simulated precipitation is biased low.

5. Discussion

Here, we summarize and further interpret the main findings of the all the numerical simulations of Typhoon

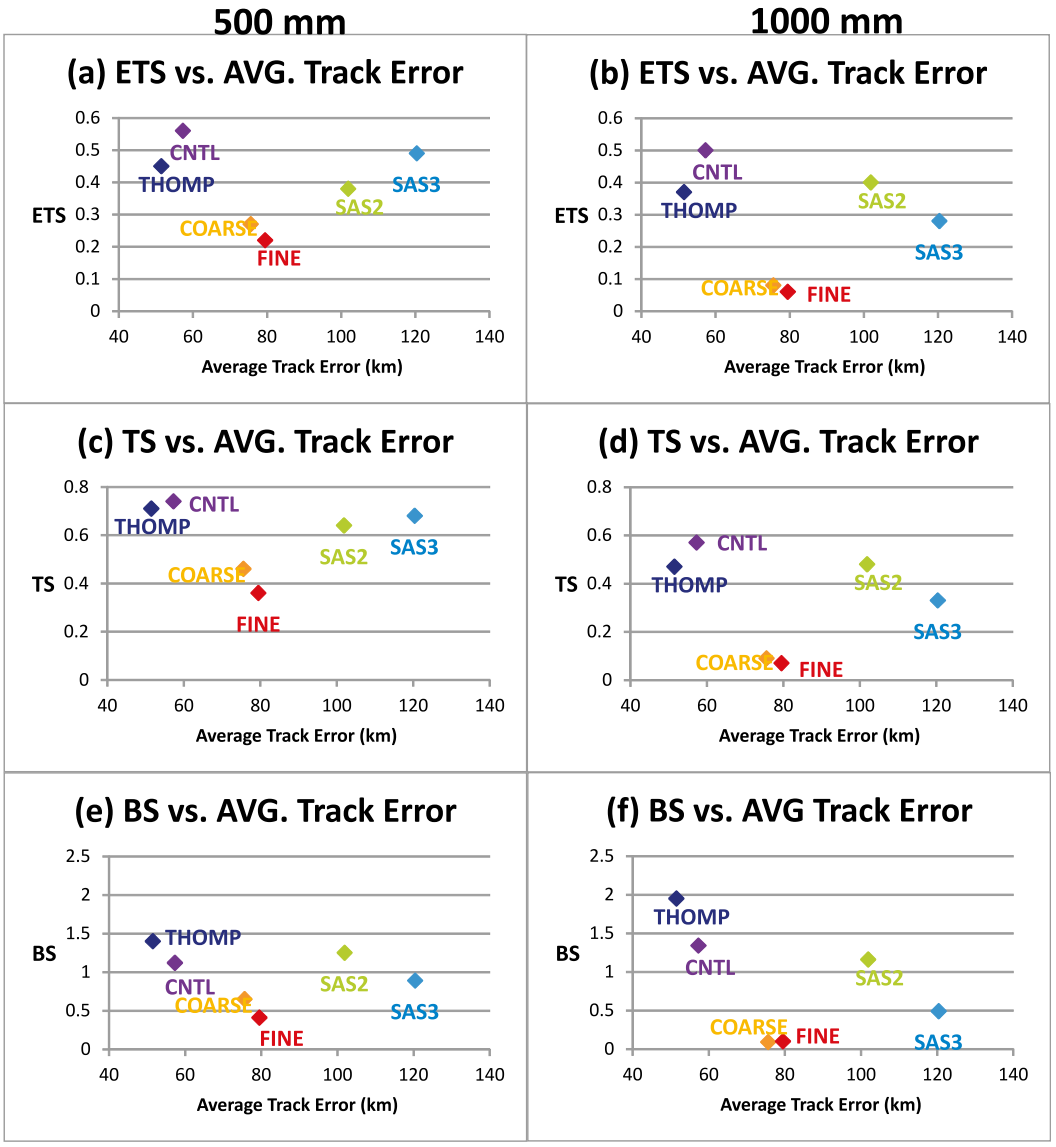

FIG. 11. QPF scores vs average track error for all of the experiments by direct comparison with the model-predicted value at the rain gauge location: (a) ETS (500 mm), (b) ETS (1000 mm), (c) TS (500 mm), (d) TS (1000 mm), (e) BS (500 mm), and (f) BS (1000 mm).

Morakot. The CNTL simulation at 5-km horizontal resolution performed the best with regard to the QPFs. There was a strong sensitivity of the QPFs as a result of varying the microphysical scheme. The THOMP simulation captured the precipitation distribution well but overpredicted the precipitation amount. With regard to the horizontal resolution sensitivity, it was demonstrated that a 15-km grid increment is not sufficient to resolve the TC-terrain interaction, leading to significant QPF errors. Both the 5- and 1.67-km simulations were sufficient to resolve this interaction. However, the variances in the mesoscale features (rainbands) between these simulations were significant, and the 1.67-km FINE simulation had a worse QPF than did the 5-km CNTL simulation. Although domain 4 (1.67 km) was large enough to cover the circulation of Morakot, it is possible that the lateral boundaries could have had some effects on the structure of the storm, particularly near the initial time (Fig. 1). Because of limited computational resources, this domain could not cover a region close to the size of domain 3, which would be necessary to fully capture the interaction of Morakot with the southwest monsoon flow. Overall, the track errors were similar between the tests with different microphysics and resolutions, and QPF differences between these simulations were due to variances in the predicted

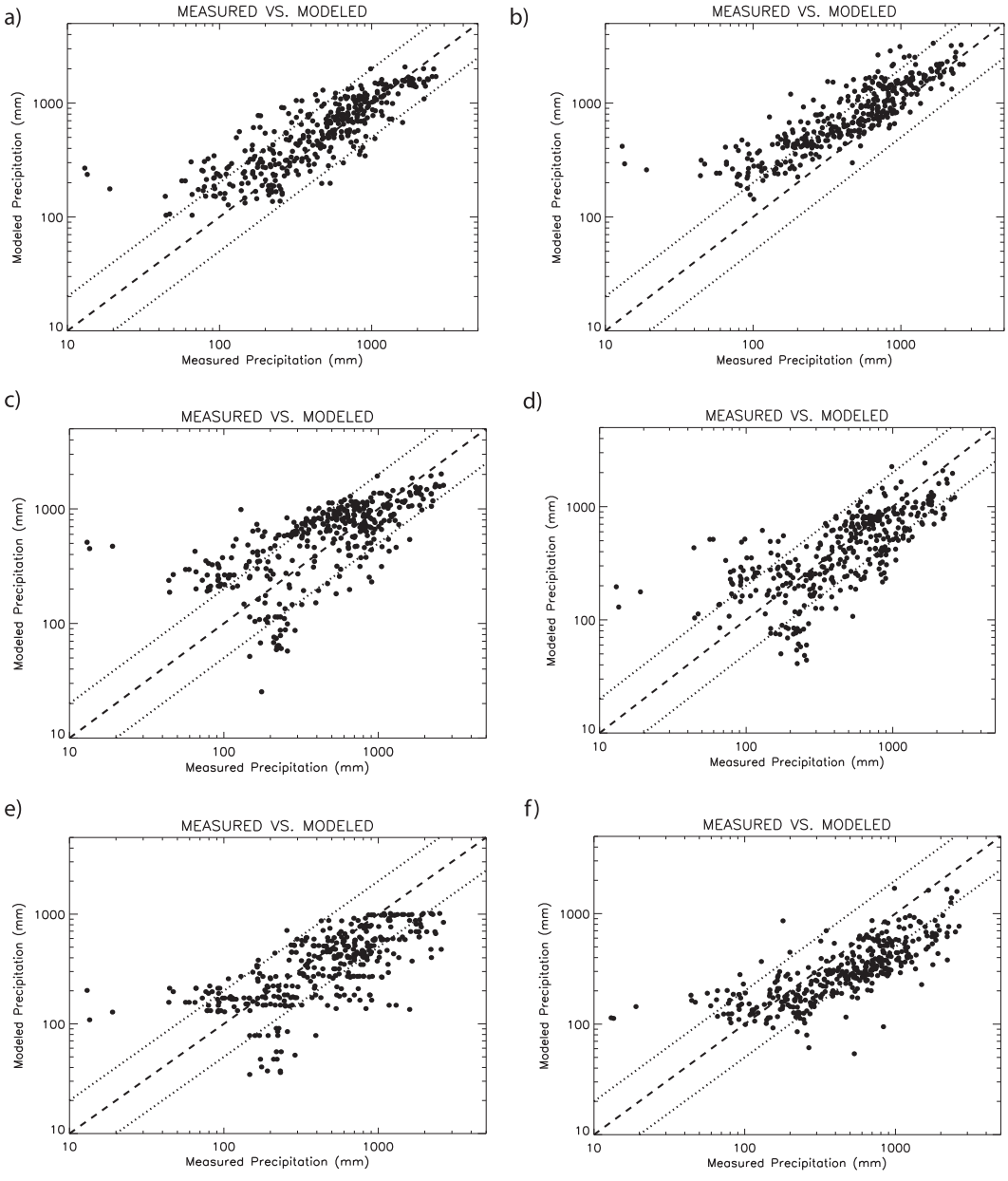

FIG. 12. Scatterplots of the measured vs modeled 3-day accumulated precipitation at the Taiwan rain gauge locations: (a) CNTL, (b) THOMP, (c) SAS2, (d) SAS3, (e) COARSE, and (f) FINE. The perfect correlation line is shown with dashes and the region of prediction within a factor of 2 is between the dotted lines.

structure and precipitation features. There was strong sensitivity of the QPFs to the cumulus parameterization. By using the SAS parameterization, Morakot was drawn too far north, causing larger QPF errors. The SAS parameterization erroneously regenerated the remnants of Goni, causing large-scale steering flow errors in Morakot. This result is consistent with the study of Sun et al. (2014), who showed significant TC track sensitivity to variances in the cumulus parameterization, modifying the large-scale environment. However, in their study, the track errors were due to the overestimation of anvil clouds away from the TC center when using a particular cumulus scheme.

6. Conclusions

Numerical simulations were conducted on Typhoon Morakot (2009) using the U.S. Navy's regional tropical cyclone prediction system, COAMPS-TC. A control simulation was executed and compared to five sensitivity

experiments. In the sensitivity tests, the microphysics, horizontal resolution, and cumulus parameterizations were varied in order to understand the effects on the track, intensity, structure, and quantitative precipitation forecast (QPF) prediction. The primary findings of this study are as follow. First, the track of Morakot was found to be relatively insensitive to variations in the horizontal resolution (15, 5, and 1.67 km) and microphysical scheme, but it was found to be quite sensitive to variations in the cumulus parameterization. A significant finding of this work is that the SAS-type cumulus parameterizations in a multiply nested TC prediction model, in some cases, can result in the erroneous generation of circulation patterns leading to modifications of the environmental steering flow. Second, the intensity was found to be relatively insensitive to the variations in horizontal resolution at convective-permitting scales (5 and 1.67 km), microphysical parameterization, and cumulus scheme (intensity errors from the cumulus scheme were due to track errors putting the storm too far north). Finally, the QPF was found to be most sensitive to changes in the horizontal resolution, microphysical parameterization, and cumulus parameterization. In particular, the changes in the horizontal resolution and microphysical parameterization modified the storm structure as it interacted with the steep terrain, leading to differences in the QPFs. Although there exists some sensitivity to these parameters, the results indicate that a multiply nested regional TC prediction model can provide an accurate QPF for large, highly asymmetric storms with multiscale interactions, such as Morakot. The enhanced predictability is likely due to the more predictable large-scale and topographic forcing.

Acknowledgments. The authors acknowledge the support of the Office of Naval Research (ONR) through Program Element (PE) 0602435N. We thank the Taiwan Central Weather Bureau for providing the rain gauge data, Greg Thompson for providing his microphysics routine, and Jim Ridout for helpful comments and discussions. We are also grateful for the computational resource and support provided by the Department of Defense (DoD) High Performance Computing Center.

REFERENCES

Arakawa, A., and W. H. Schubert, 1974: Interaction of a cumulus cloud ensemble with the large-scale environment, Part I. *J. Atmos. Sci.*, **31**, 674–701, doi:10.1175/1520-0469(1974)031<0674:IOACCE>2.0.CO;2.

Chan, J. C. L., and W. M. Gray, 1982: Tropical cyclone movement and surrounding flow relationships. *Mon. Wea. Rev.*, **110**, 1354–1374, doi:10.1175/1520-0493(1982)110<1354:TCMASF>2.0.CO;2.

Chen, S., and Coauthors, 2003: COAMPS version 3 model description: General theory and equations. Naval Research Laboratory Tech. Rep. NRL/PU7500-04-448, 141 pp.

Chien, F.-C., and H.-C. Kuo, 2011: On the extreme rainfall of Typhoon Morakot (2009). *J. Geophys. Res.*, **116**, D05104, doi:10.1029/2010JD015092.

Colle, B. A., K. J. Westrick, and C. F. Mass, 1999: Evaluation of MM5 and Eta-10 precipitation forecasts over the Pacific Northwest during the cool season. *Wea. Forecasting*, **14**, 137–154, doi:10.1175/1520-0434(1999)014<0137:EOMAEP>2.0.CO;2.

Daley, R., and E. Barker, 2001: NAVDAS: Formulation and diagnostics. *Mon. Wea. Rev.*, **129**, 869–883, doi:10.1175/1520-0493(2001)129<0869:NFAD>2.0.CO;2.

Donelan, M. A., B. K. Haus, N. Reul, W. J. Plant, M. Stiassnie, and H. C. Graber, 2004: On the limiting aerodynamic roughness of the ocean in very strong winds. *Geophys. Res. Lett.*, **31**, L18306, doi:10.1029/2004GL019460.

Doyle, J. D., and Coauthors, 2011: Real-time tropical cyclone prediction using COAMPS-TC. *Atmospheric Science (AS) & Ocean Science (OS)*, K. Satake, Ed., Advances in Geosciences, Vol. 28, World Scientific, 15–28.

——, and Coauthors, 2014: Tropical cyclone prediction using COAMPS-TC. *Oceanography*, **27**, 104–115, doi:10.5670/oceanog.2014.72.

Evans, J. L., G. L. Holland, and R. L. Elsberry, 1991: Interactions between a barotropic vortex and an idealized subtropical ridge. Part I: Vortex motion. *J. Atmos. Sci.*, **48**, 301–314, doi:10.1175/1520-0469(1991)048<0301:IBABVA>2.0.CO;2.

Fang, X., and Y.-H. Kuo, 2013: Improving ensemble-based quantitative precipitation forecasts for topography-enhanced typhoon heavy rainfall over Taiwan with a modified probability-matching technique. *Mon. Wea. Rev.*, **141**, 3908–3932, doi:10.1175/MWR-D-13-00012.1.

——, ——, and A. Wang, 2011: The impacts of Taiwan topography on the predictability of Typhoon Morakot's record-breaking rainfall: A high-resolution ensemble simulation. *Wea. Forecasting*, **26**, 613–633, doi:10.1175/WAF-D-10-05020.1.

Fu, Q., and K. N. Liou, 1993: Parameterization of the radiative properties of cirrus clouds. *J. Atmos. Sci.*, **50**, 2008–2025, doi:10.1175/1520-0469(1993)050<2008:POTRPO>2.0.CO;2.

Hall, J. D., M. Xue, L. Ran, and L. M. Leslie, 2013: High-resolution modeling of Typhoon Morakot (2009): Vortex Rossby waves and their role in extreme precipitation over Taiwan. *J. Atmos. Sci.*, **70**, 163–186, doi:10.1175/JAS-D-11-0338.1.

Han, J., and H.-L. Pan, 2011: Revision of convection and vertical diffusion schemes in the NCEP Global Forecast System. *Wea. Forecasting*, **26**, 520–533, doi:10.1175/WAF-D-10-05038.1.

Hendricks, E. A., J. R. Moskaitis, Y. Jin, R. M. Hodur, J. D. Doyle, and M. S. Peng, 2011: Prediction and diagnosis of Typhoon Morakot (2009) using the Naval Research Laboratory's mesoscale tropical cyclone model. *Terr. Atmos. Oceanic Sci.*, **22**, 579–594, doi:10.3319/TAO.2011.05.30.01(TM).

Hodur, R. M., 1997: The Naval Research Laboratory's Coupled Ocean/Atmosphere Mesoscale Prediction System (COAMPS). *Mon. Wea. Rev.*, **125**, 1414–1430, doi:10.1175/1520-0493(1997)125<1414:TNRLSC>2.0.CO;2.

Hogan, T. F., and T. E. Rosmond, 1991: The description of the Navy Operational Global Atmospheric Prediction System's spectral forecast model. *Mon. Wea. Rev.*, **119**, 1786–1815, doi:10.1175/1520-0493(1991)119<1786:TDOTNO>2.0.CO;2.

Jin, Y., W. T. Thompson, S. Wang, and C.-S. Liou, 2007: A numerical study of the effect of dissipative heating on tropical cyclone intensity. *Wea. Forecasting*, **22**, 950–966, doi:10.1175/WAF1028.1.

——, and Coauthors, 2014: The impact of ice phase cloud parameterizations on tropical cyclone prediction. *Mon. Wea. Rev.*, **142**, 606–625, doi:10.1175/MWR-D-13-00058.1.

Kain, J. S., 2004: The Kain–Fritsch convective parameterization: An update. *J. Appl. Meteor. Climatol.*, **43**, 170–181, doi:10.1175/1520-0450(2004)043<0170:TKCPAU>2.0.CO;2.

——, and J. M. Fritsch, 1990: A one-dimensional entraining/detraining plume model and its application in convective parameterization. *J. Atmos. Sci.*, **47**, 2784–2802, doi:10.1175/1520-0469(1990)047<2784:AODEPM>2.0.CO;2.

——, and ——, 1993: Convective parameterization for mesoscale models: The Kain–Fritsch scheme. *The Representation of Cumulus Convection in Numerical Models*, *Meteor. Monogr.*, No. 46, Amer. Meteor. Soc., 165–170.

Klemp, J. B., and R. B. Wilhelmson, 1978: The simulation of three-dimensional convective storm dynamics. *J. Atmos. Sci.*, **35**, 1070–1096, doi:10.1175/1520-0469(1978)035<1070:TSOTDC>2.0.CO;2.

Liang, J., L. Wu, X. Ge, and C.-C. Wu, 2011: Monsoonal influence on Typhoon Morakot (2009). Part II: Numerical study. *J. Atmos. Sci.*, **68**, 2222–2235, doi:10.1175/2011JAS3731.1.

Lin, Y.-L., R. D. Farley, and H. D. Orville, 1983: Bulk parameterization of the snow field in a cloud model. *J. Climate Appl. Meteor.*, **22**, 1065–1092, doi:10.1175/1520-0450(1983)022<1065:BPOTSF>2.0.CO;2.

Liou, C.-S., and K. D. Sashegyi, 2011: On the initialization of tropical cyclones with a three-dimensional variational analysis. *Nat. Hazards*, **63**, 1375–1391, doi:10.1007/s11069-011-9838-0.

Mellor, G. L., and T. Yamada, 1982: Development of a turbulence closure for geophysical fluid problems. *Rev. Geophys. Space Phys.*, **20**, 851–875, doi:10.1029/RG020i004p00851.

Nguyen, H. V., and Y.-L. Chen, 2011: High resolution initialization and simulations of Typhoon Morakot (2009). *Mon. Wea. Rev.*, **139**, 1463–1491, doi:10.1175/2011MWR3505.1.

Pan, H.-L., and W.-S. Wu, 1995: Implementing a mass flux convective parameterization package for the NMC medium-range forecast model. NMC Office Note 409, 40 pp. [Available online at http://www.lib.ncep.noaa.gov/ncepofficenotes/files/01408A42.pdf.]

Rutledge, S. A., and P. V. Hobbs, 1983: The mesoscale and microscale structure and organization of clouds and precipitation in midlatitude cyclones. VIII: A model for the seeder-feeder process in warm-frontal rainbands. *J. Atmos. Sci.*, **40**, 1185–1206, doi:10.1175/1520-0469(1983)040<1185:TMAMSA>2.0.CO;2.

Schwartz, C. S., Z. Liu, Y. Chen, and X.-Y. Huang, 2012: Impact of assimilating microwave radiances with a limited-area ensemble data assimilation system on forecasts of Typhoon Morakot. *Wea. Forecasting*, **27**, 424–437, doi:10.1175/WAF-D-11-00033.1.

Sun, Y., Z. Zhong, W. Lu, and Y. Hu, 2014: Why are tropical cyclone tracks over the western North Pacific sensitive to the cumulus parameterization scheme in regional climate modeling? A case study for Megi (2010). *Mon. Wea. Rev.*, **142**, 1240–1249, doi:10.1175/MWR-D-13-00232.1.

Thompson, G., R. M. Rasmussen, and K. Manning, 2008: Explicit forecasts of winter precipitation using an improved bulk microphysics scheme. Part II: Implementation of a new snow parameterization. *Mon. Wea. Rev.*, **136**, 5095–5115, doi:10.1175/2008MWR2387.1.

Wang, C.-C., 2014: On the calculation and correction of equitable threat score for model quantitative precipitation forecasts for small verification areas: The example of Taiwan. *Wea. Forecasting*, **29**, 788–798, doi:10.1175/WAF-D-13-00087.1.

——, H.-C. Kuo, Y.-H. Chen, H.-L. Huang, C.-H. Chung, and K. Tsuboki, 2012: Effects of asymmetric latent heating on typhoon movement crossing Taiwan: The case of Morakot (2009) with extreme rainfall. *J. Atmos. Sci.*, **69**, 3172–3196, doi:10.1175/JAS-D-11-0346.1.

Wu, C.-C., 2013: Typhoon Morakot: Key findings from the journal *TAO* for improving prediction of extreme rains at landfall. *Bull. Amer. Meteor. Soc.*, **94**, 155–160, doi:10.1175/BAMS-D-11-00155.1.

——, and Y.-H. Kuo, 1999: Typhoons affecting Taiwan: Currently understanding and future challenges. *Bull. Amer. Meteor. Soc.*, **80**, 67–80, doi:10.1175/1520-0477(1999)080<0067:TATCUA>2.0.CO;2.

——, T.-H. Yen, Y.-H. Kuo, and W. Wang, 2002: Rainfall simulation associated with Typhoon Herb (1996) near Taiwan. Part I: The topographic effect. *Wea. Forecasting*, **17**, 1001–1015, doi:10.1175/1520-0434(2003)017<1001:RSAWTH>2.0.CO;2.

Wu, L., J. Liang, and C.-C. Wu, 2011: Monsoonal influence on Typhoon Morakot (2009). Part I: Observational analysis. *J. Atmos. Sci.*, **68**, 2208–2221, doi:10.1175/2011JAS3730.1.

Xie, B., and F. Zhang, 2012: Impacts of typhoon track and island topography on the heavy rainfalls in Taiwan associated with Morakot (2009). *Mon. Wea. Rev.*, **140**, 3379–3394, doi:10.1175/MWR-D-11-00240.1.

Yen, T.-H., C.-C. Wu, and G.-Y. Lien, 2011: Rainfall simulations of Typhoon Morakot with controlled translation speed based on EnKF data assimilation. *Terr. Atmos. Oceanic Sci.*, **22**, 647–660, doi:10.3319/TAO.2011.07.05.01(TM).